

Analysis of LS-DYNA MOR Approaches for Application in Crash Analysis and Integration in SDM Workflows

Zeidoun El Khatib¹, Uwe Reuter¹, Marko Thiele²

¹TU Dresden
²SCALE GmbH

1 Introduction

1.1 Motivation

Numerical simulations are often characterized by long computational times, especially as the size of the model grows larger. In many cases, this necessitates the use of a high-performance computer in order to speed up the simulation and obtain results faster. Nevertheless, computational times can still be large, such as in the automotive and aerospace industries.

The automotive industry is highly dependent on numerical modelling. Companies perform numerical simulations for crash analysis in the preliminary phases of design, because it eliminates the need to perform expensive physical crash tests of prototypes. Optimization, another time-consuming process, is also often performed during the different stages of a project and is only possible using virtual testing. However, optimization adds to the scale of computational time needed in the automotive industry for virtual product development. The longer it takes to perform such numerical processes, the longer the time-to-market of a certain vehicle model and eventually, the higher the cost.

1.2 Goal

In order to overcome such challenges, some techniques known as model order reduction (MOR) are used. Many of these techniques can be applied to structural systems exhibiting geometric, material, and boundary linearities, while some aim to handle systems characterised by such non-linearities and are often empowered by algorithms that help detect such nonlinearities.

This work aims to assess some linear MOR techniques in vehicle simulation. In particular, methods available within the finite element software LS-DYNA were applied in the context of a crash analysis. These methods were first evaluated on a structural frame exhibiting dynamic behaviour. The knowledge obtained about these methods was then transferred to a side impact crash scenario. The efficiency of these methods with regards to time and accuracy was evaluated in both examples. Based on the evaluation, a decision was made regarding their applicability and what would be the restrictions to their usage. Based on the findings of this work, it is believed that the research done can be taken a step further in order to find more guidelines for the usage of LS-DYNA's model order reduction approaches, that help optimize their definition and performance. In addition, this work addresses the integration of MOR into simulation using simulation data management (SDM).

2 Model Order Reduction

MOR techniques are useful tools available in different scientific fields. They were originally developed in control and systems theory [1]. The properties of a dynamical system are studied, after which its complexity is aimed to be reduced while maintaining the input-output behaviour of the system as much as possible.

MOR aims to simplify large dynamical models in order to speed up the calculation process and reduce storage requirements, while maintaining a reasonable accuracy. A dynamical model may contain many equations and/or variables. These equations tend to be complicated ones such as coupled first order differential equations. As the number of these equations increases, the complexity of the model increases and sometimes a solution is not even feasible. An MOR method aims to restrict the number of these equations/variables, while capturing the essential features of the system, in order to simplify the solution step. The theory of MOR in relation to structural dynamics system, i.e., second order systems, is explained in the following. The interested reader is referred to [2] for a detailed formulation of MOR for first order systems.

The dynamics of a linear structural system are represented by a system of linear second-order differential equations, explicitly through the equation of motion (EOM), as

$$\mathbf{M}\ddot{\underline{x}}(t) + \mathbf{C}\dot{\underline{x}}(t) + \mathbf{K}\underline{x}(t) = \underline{f}(t) \quad (1)$$

where \mathbf{M}, \mathbf{C} , and $\mathbf{K} \in \mathbb{R}^{n \times n}$ are the system's mass, damping, and stiffness matrices respectively, $\ddot{\underline{x}}(t), \dot{\underline{x}}(t), \underline{x}(t)$, and $\underline{f}(t) \in \mathbb{R}^n$ are the acceleration, velocity, displacement, and external load vectors respectively, and n is the number of degrees of freedom (DoFs) of the full original structural system. In the absence of damping the EOM reduces to

$$\mathbf{M}\ddot{\underline{x}}(t) + \mathbf{K}\underline{x}(t) = \underline{f}(t) \quad (2)$$

An MOR technique aims to find a transformation $\mathbf{T} \in \mathbb{R}^{n \times k}$ that transforms the reduced vector of displacements $\underline{x}_k(t)$ from the reduced space to the full vector of displacements $\underline{x}(t)$ in the original space as follows

$$\underline{x}(t) = \mathbf{T}\underline{x}_k(t) \quad (3)$$

where k is the size of the reduced system and $k \ll n$. Depending on the method of choice, this transformation has a different formulation, yet the same role. For a linear time-invariant system, the transformation is time independent and it follows

$$\dot{\underline{x}}(t) = \mathbf{T}\dot{\underline{x}}_k(t) \quad (4)$$

$$\ddot{\underline{x}}(t) = \mathbf{T}\ddot{\underline{x}}_k(t) \quad (5)$$

Inserting these relations into the EOM yields

$$\mathbf{M}\mathbf{T}\ddot{\underline{x}}_k(t) + \mathbf{C}\mathbf{T}\dot{\underline{x}}_k(t) + \mathbf{K}\mathbf{T}\underline{x}_k(t) = \underline{f}(t) \quad (6)$$

Multiplying the equation by \mathbf{T}^T from the left side yields

$$\mathbf{T}^T\mathbf{M}\mathbf{T}\ddot{\underline{x}}_k(t) + \mathbf{T}^T\mathbf{C}\mathbf{T}\dot{\underline{x}}_k(t) + \mathbf{T}^T\mathbf{K}\mathbf{T}\underline{x}_k(t) = \mathbf{T}^T\underline{f}(t) \quad (7)$$

written in a simplified form

$$\mathbf{M}_k\ddot{\underline{x}}_k(t) + \mathbf{C}_k\dot{\underline{x}}_k(t) + \mathbf{K}_k\underline{x}_k(t) = \underline{f}_k(t) \quad (8)$$

where each system matrix \square_k is obtained as $\square_k = \mathbf{T}^T\square\mathbf{T}$ and the reduced vector of external forces $\underline{f}_k(t)$ as $\underline{f}_k(t) = \mathbf{T}^T\underline{f}(t)$. By solving this reduced system of equations, the reduced vector of displacements $\underline{x}_k(t)$ is obtained, from which the full vector of displacements $\underline{x}(t)$ can be approximated and reconstructed using the transformation \mathbf{T} as $\underline{x}(t) = \mathbf{T}\underline{x}_k(t)$.

There exist different MOR methods which handle linear and non-linear (geometry, material, and boundary) behaviour. Methods handling linearity are much more mature and have been around for a long time. The fundamental methods were published in the eighties and nineties of the last century [1]. However, there are sub-structuring methods and techniques that date back to the sixties such as *Guyan Condensation* and *Craig-Bampton*. The method of *Truncated Balanced Realization* was published by Moore in 1981 while the *Proper Orthogonal Decomposition* method was proposed by Sirovich in 1987; both for the sake of system and control theory field [1]. *Krylov subspace* methods were born in the nineties with the first method being *Asymptotic Waveform Evaluation* in 1990. Other methods followed and many others are still being improved and researched specially to handle non-linearities.

Although, a crash exhibits several non-linearities, there exist large portions of the vehicle that behave linearly, thus are candidates for linear MOR. From this viewpoint, it is still worth considering linear MOR in crashworthiness. After all, linear methods are well understood and have been used for decades, while the non-linear ones are still being improved and encounter a lot of constraints and restrictions. Parts that behave linearly can be reduced in order to speed up the calculations.

2.1 Modal Truncation

A dynamic structural system is differential and coupled by nature. This renders the solution of such systems tedious and cumbersome. Therefore, the need to decouple the system and ease the solution process arises. A modal matrix is used to do so and produce a set of independent equations, which is known as the classical meaning of *modal analysis* [3]. Modal analysis also refers to the calculation of modal parameters including natural frequency, natural mode, damping factor, etc.

The theory of vibration states that for a time-invariant system, the responses can be obtained as a linear combination of all the responses in the normal space (i.e., the modal space formed by the normalized eigenvectors) [3]. This linear combination is nothing more than a superposition, hence the name *mode superposition* or *modal superposition* arises. In a system with n DoFs, there exists n eigenvalues and n eigenmodes¹. Considering the i^{th} DoF, one can obtain its displacement using a superposition of the eigenmode values of this DoF as follows

$$x_i(t) = \varphi_{i1}q_1(t) + \varphi_{i2}q_2(t) + \dots + \varphi_{in}q_n(t) = \sum_{m=1}^n \varphi_{im}q_m(t) \quad (9)$$

where $\varphi_{i1}, \varphi_{i2}, \dots, \varphi_{in}$ are the displacements of the i^{th} DoF in the 1st, 2nd, ..., n^{th} eigenmodes (eigenvectors) respectively, $q_1(t), q_2(t), \dots, q_n(t)$ are the modal coordinates which represent the response in the modal space, and m is the index of the eigenmode in the set of n eigenmodes.

The displacement vector of the full order model (FOM) is thus obtained as

$$\underline{x}(t) = \Phi \underline{q}(t) = \sum_{m=1}^n \varphi_m q_m(t) \quad (10)$$

with

$$\underline{q}(t) = [q_1(t) \quad q_2(t) \quad \dots \quad q_n(t)]^T \quad (11)$$

Inserting the mode superposition equation into the undamped EOM yields the decoupled system of equations

$$\ddot{\underline{q}}(t) + \Lambda \underline{q}(t) = \Phi^T \underline{f}(t) \quad (12)$$

FEM models are usually large (thousands or millions of DoFs), so extracting all modes is not practical and also impossible, besides that error arises as the number of modes increases [3]. Furthermore, each mode contributes differently to the response based on its corresponding eigenfrequency and the external excitation. If the mode has a frequency close to the excitation frequency it would be activated. Often, the frequency content of exciting forces has an upper limit so the modes that have an eigenfrequency larger than this limit will not be well excited and hence contribute minimally to the response [3]. Therefore, it is possible to ignore these modes without a major loss of accuracy; the eigenmodes are truncated and the method is referred to as modal truncation. Not only does it save time in the modal analysis but also in solving the model.

The extraction of the first k modes yields the displacement of the reduced order model (ROM)

$$\underline{x}(t) \approx \Phi_k \underline{q}_k(t) = \sum_{m=1}^k \varphi_m q_m(t) \quad k \ll n \quad (13)$$

2.2 Component Mode Synthesis and Sub-structuring

Component mode synthesis (CMS), also known as dynamic sub-structuring, has quite a history in MOR. It is one of the most popular methods used in large structural models and is frequently used in dynamic analysis. There are two main reasons behind that [4]. First, low frequency modes are usually our interest and hence it makes sense to reduce from the start the EVP. It is worth mentioning that CMS works well for low frequency modes of a system but do not perform well for mid- to high-frequency modes [5]. Second, large projects are usually divided into several parts in order to allow different teams or even companies to handle them, to speed up the design process. Each subdivided part has its own model which is later integrated into the full one. Such subdivision is called sub-structuring [4].

There are several approaches that fall under CMS. These techniques focus on the reduction of the interior DoFs of each substructure while retaining all physical DoFs at the interfaces, making the assembly process after that straightforward [5]. These techniques differ by how they handle the interface and consequently the definition of the reduction matrix that projects the model into the reduced space. There are fixed interface methods such as Craig-Bampton, free-interface method such as those by Goldman (1969) and Hou (1969), and hybrid methods such as MacNeal (1971) [4,5].

2.2.1 Guyan Condensation

Guyan condensation is one of the oldest MOR techniques. It dates back to 1965 and was proposed by Guyan and Irons. It targets deleting unwanted DoFs and since it ignores the dynamic effects of the system, it is also called static condensation (SC) [3]. Starting from the undamped inhomogeneous EOM

¹ There is a possibility that some eigenvalues are not distinct, however the principle is the same.

the system of equations is split into two parts. The first part represents the DoFs at the boundary, i.e. interface, and the second part reflects the internal DoFs. Different literature provides different notations for such a split. For instance, [3] uses the subscripts m (master) and s (slave) respectively. The master being the boundary DoFs while the slaves are the internal ones. Since the internal DoFs are related to the boundary ones, they are their slaves. On the other hand, [4] refers to them as r (remaining) and c (condensed) respectively, while [6] refers to them as b (boundary) and i (internal) respectively. In this work, the last notation is adopted. The system of equations becomes

$$\begin{bmatrix} \mathbf{M}_{bb} & \mathbf{M}_{bi} \\ \mathbf{M}_{ib} & \mathbf{M}_{ii} \end{bmatrix} \begin{bmatrix} \ddot{\underline{x}}_b(t) \\ \ddot{\underline{x}}_i(t) \end{bmatrix} + \begin{bmatrix} \mathbf{K}_{bb} & \mathbf{K}_{bi} \\ \mathbf{K}_{ib} & \mathbf{K}_{ii} \end{bmatrix} \begin{bmatrix} \underline{x}_b(t) \\ \underline{x}_i(t) \end{bmatrix} = \begin{bmatrix} \underline{f}_b(t) \\ \underline{f}_i(t) \end{bmatrix} \quad (14)$$

The aim is to find a relation between the internal DoFs and the external ones. By taking the second equation set of the above system, and assuming no forces are applied at the internal DoFs, we obtain

$$\mathbf{M}_{ib}\ddot{\underline{x}}_b(t) + \mathbf{M}_{ii}\ddot{\underline{x}}_i(t) + \mathbf{K}_{ib}\underline{x}_b(t) + \mathbf{K}_{ii}\underline{x}_i(t) = \underline{0} \quad (15)$$

Setting the accelerations equal to $\underline{0}$, i.e., ignoring the dynamic effects, the equation reduces to

$$\mathbf{K}_{ib}\underline{x}_b(t) + \mathbf{K}_{ii}\underline{x}_i(t) = \underline{0} \quad (16)$$

$$\underline{x}_i(t) = -\mathbf{K}_{ii}^{-1}\mathbf{K}_{ib}\underline{x}_b(t) \quad (17)$$

$$\underline{x}_i(t) = \mathbf{R}_G\underline{x}_b(t) \quad (18)$$

where $\mathbf{R}_G \in \mathbb{R}^{ixb}$ is the condensation matrix relating the internal displacements to the boundary ones. The vector of displacements can now be reconstructed as

$$\underline{x}(t) = \begin{bmatrix} \underline{x}_b(t) \\ \underline{x}_i(t) \end{bmatrix} = \begin{bmatrix} \mathbf{I} \\ \mathbf{R}_G \end{bmatrix} \underline{x}_b(t) = \mathbf{T}_G\underline{x}_b(t) \quad (19)$$

where $\mathbf{T}_G = \begin{bmatrix} \mathbf{I} \\ \mathbf{R}_G \end{bmatrix} \in \mathbb{R}^{n \times b}$ is the coordinate transformation matrix or the global mapping matrix that relates the vector of displacements to the boundary ones, and $\mathbf{I} \in \mathbb{R}^{b \times b}$ is the identity matrix.

$$\mathbf{M}_k\ddot{\underline{x}}_b(t) + \mathbf{K}_k\underline{x}_b(t) = \underline{f}_k(t) \quad (20)$$

follows, where

$$\mathbf{M}_k = \mathbf{M}_{bb} + \mathbf{K}_{bi}\mathbf{K}_{ii}^{-1}\mathbf{M}_{ii}\mathbf{K}_{ii}^{-1}\mathbf{K}_{ib} - \mathbf{K}_{bi}\mathbf{K}_{ii}^{-1}\mathbf{M}_{ib} - \mathbf{M}_{bi}\mathbf{K}_{ii}^{-1}\mathbf{K}_{ib} \quad (21)$$

$$\mathbf{K}_k = \mathbf{K}_{bb} - \mathbf{K}_{bi}\mathbf{K}_{ii}^{-1}\mathbf{K}_{ib} \quad (22)$$

$$\underline{f}_k(t) = \underline{f}_b(t) - \mathbf{K}_{bi}\mathbf{K}_{ii}^{-1}\underline{f}_i(t) \quad (23)$$

Since the Guyan condensation matrix was obtained from the dynamic equations by ignoring the dynamic effects, an error is introduced when the dynamic problem is considered. The magnitude of such an error depends on the natural properties of the full model and how many and what DoF are selected as the masters [3]. If the problem is static, this method yields desirable results. Solving the equilibrium system, one obtains the vector of displacements at the boundaries. The full vector of displacements can then be approximated. Solving the reduced system of equations leads to computational savings.

2.2.2 Craig Bampton

Craig Bampton (CB), also referred to by some as Hurty-Craig-Bampton aims to overcome the limitations of static condensation by taking into account the inertia effects that could be partially or fully included in the condensation. By taking these effects into account, the reduction becomes dynamic; hence the name. The method is based on collecting both the static and internal vibration (dynamic) modes. Static modes result from applying unit displacements on the boundary DoFs (this is static condensation) whereas vibration modes are those induced in the structure by external excitations while having its boundaries fixed.

In contrast to static condensation, where a relation between the internal displacements and boundary ones leads to the desired relation between the vector of displacements and the boundary ones, dynamic substructuring is founded on the relation between the displacements vector \underline{x} and the coordinates of the reduced model \underline{p} , which consists of the boundary displacements \underline{x}_b and the generalized coordinates \underline{q}_k [3]. Hence, the boundary displacements aren't solely responsible for the relation.

Starting from

$$\begin{bmatrix} \mathbf{M}_{bb} & \mathbf{M}_{bi} \\ \mathbf{M}_{ib} & \mathbf{M}_{ii} \end{bmatrix} \begin{bmatrix} \ddot{\underline{x}}_b(t) \\ \ddot{\underline{x}}_i(t) \end{bmatrix} + \begin{bmatrix} \mathbf{K}_{bb} & \mathbf{K}_{bi} \\ \mathbf{K}_{ib} & \mathbf{K}_{ii} \end{bmatrix} \begin{bmatrix} \underline{x}_b(t) \\ \underline{x}_i(t) \end{bmatrix} = \begin{bmatrix} \underline{f}_b(t) \\ \underline{f}_i(t) \end{bmatrix} \quad (24)$$

the Craig-Bampton transformation is defined as

$$\underline{x}(t) = \begin{bmatrix} \underline{x}_b(t) \\ \underline{x}_i(t) \end{bmatrix} = \begin{bmatrix} \mathbf{I} & \mathbf{0} \\ \mathbf{\Phi}_c & \mathbf{\Phi}_k \end{bmatrix} \begin{bmatrix} \underline{x}_b(t) \\ \underline{q}_k(t) \end{bmatrix} = [\hat{\mathbf{\Phi}}_c \quad \hat{\mathbf{\Phi}}_k] \begin{bmatrix} \underline{x}_b(t) \\ \underline{q}_k(t) \end{bmatrix} = \mathbf{T} \underline{p}(t) \quad (25)$$

where $\mathbf{\Phi}_c = -\mathbf{K}_{ii}^{-1}\mathbf{K}_{ib}$, $\hat{\mathbf{\Phi}}_c$ is the constraint modes matrix, equivalent to the coordinate transformation matrix \mathbf{T}_G in static condensation, and $\hat{\mathbf{\Phi}}_k$ is the component mass normalized modes matrix obtained from the following eigenvalue-problem

$$\mathbf{K}_{ii}\mathbf{\Phi}_{ii} = \mathbf{M}_{ii}\mathbf{\Phi}_{ii}\mathbf{\Lambda}_{ii} \quad (26)$$

The columns of $\mathbf{\Phi}_k$ are the (selected) eigenmodes of the substructure obtained using fixed interface boundaries. Therefore, they are called the fixed interface modes. Inserting the displacement and acceleration vectors into the EOM yields

$$\begin{bmatrix} \mathbf{M}_{bb} & \mathbf{M}_{bk} \\ \mathbf{M}_{kb} & \mathbf{I}_{kk} \end{bmatrix} \ddot{\underline{p}}(t) + \begin{bmatrix} \mathbf{K}_{bb} & \mathbf{0} \\ \mathbf{0} & \mathbf{\Lambda}_{kk} \end{bmatrix} \underline{p}(t) = \begin{bmatrix} \underline{f}_b(t) \\ \underline{f}_k(t) \end{bmatrix} \quad (27)$$

The reader is referred to [3] for the detailed formulation of the mass and stiffness matrices involved.

2.3 MOR using LS-DYNA

In order to understand the MOR methods in LS-DYNA, it is essential to distinguish between eigenmodes, constraint modes, and attachment modes. This is due to the fact that their usage dictates the reduction process. Eigenmodes represent the natural response of a system to external frequency excitations and are obtained by solving the eigenvalue-problem of the system. The frequencies obtained represent the natural frequencies (excitations) that can put the system in a vibration state. Each excitation leads to a certain deformation pattern represented by the eigenvector (eigenmode vector). Plotting these vectors provides the vibration shape of a structure due to a particular excitation. If the body or structure is free from constraints, the calculated modes would also include rigid-body-motion.

Constraint modes, on the other hand, help capture the motions of a particular set of points. They introduce a full spectrum of frequency since they can capture motions that are not necessarily captured by the lowest extracted eigenmodes [7]. They are obtained by applying unit displacements at the boundary DoFs, one at a time, and evaluating the response at the other DoFs. Introducing constraint modes in the ROM can substantially reduce the stable time step size [7]. Recalling the definition of the allowable time step $\Delta t \leq \frac{2}{\omega_{max}}$, the frequencies resulting from the constraint modes can be so high yielding a very small time step. This eventually increases the computational costs and can counteracts the benefits of MOR.

Attachment modes are similar to constraint modes, but they introduce response where sensors or other models are to be attached [7]. They also introduce a full frequency spectrum that can limit the time step significantly. A defined set of DoFs would have its modes calculated by applying a unit load at each DoF, one at a time while the other DoFs have zero forces, and finding the response at all other DoFs [7, 8]. The assembly of such responses forms the attachment modes matrix. Due to the non-diagonal nature of the constraint and attachment mode matrices, the resulting system is coupled and the solution of the EOM becomes more complicated [7, 9].

2.3.1 Superelement

“A superelement is a group of finite elements in which part of the degrees of freedom is condensed out for computational and modelling purposes” [3]. It can have an arbitrary shape, size, and material properties contrary to a regular mesh that would be formed of elements having a more or less regular simple shapes [3]. The boundary nodes are preserved in order to be attached to the complete model later on.

Linear elastic substructures can be represented using stiffness matrices referred to as SE. By reducing the number of DoFs of the SE before incorporating it into the full model, the calculation time can be reduced. The size of the SE stiffness matrix is thus determined by the number of DoFs retained.

Depending on how well the selected DoFs represent the displacements of the actual substructure, the accuracy of the solution will be influenced [7].

The SE can be formed using either static condensation or Craig-Bampton. There are two options in LS-DYNA to form an SE using static condensation. The first is using ***CONTROL_IMPLICIT_STATIC_CONDENSATION**. The nodes to be preserved shall be defined in a node set which is referenced using **SC_NSID**. The other option is to use the ***CONTROL_IMPLICIT_MODES** card with only the constraint modes being defined. If the SE is to be formed using Craig-Bampton reduction, ***CONTROL_IMPLICIT_MODES** shall be defined using the eigenmodes and constraint modes. The user shall define the name of the SE using **SE_FILENAME**. This name is used with the ***ELEMENT_DIRECT_MATRIX_INPUT** card to import the SE into the ROM. The SE formation is done implicitly, thus the following implicit cards shall be used: ***CONTROL_IMPLICIT_GENERAL**, ***CONTROL_TERMINATION**, and ***CONTROL_IMPLICIT_SOLVER**.

Using the SE approach requires some care. First, the parts that are reduced into a SE shall be carefully deleted from the model ensuring that no elements are present as reduced and unreduced simultaneously. Forming the SE requires double precision and an SMP LS-DYNA version (at least by the time this work was written). In addition, a SE can't be mass scaled, hence the time step can't be user-manipulated when the model includes a SE.

2.3.2 *Linearized Flexible Body*

The concept of Linearized Flexible Body (LFB) was introduced back in 2002. An LFB is also referred to as Flexible Rigid Body by [7] and Deformable Rigid Body by [9, 10]. The traditional modal analysis, on which the SE approach is established, is based on the principle of modal superposition, which restricts the usage of traditional modal analysis to problems with small strains and small displacements [7]. In order to overcome such restrictions, LFB was introduced. "Unlike superelements, linearized flexible bodies are accurate for systems undergoing large displacements and large rotations" [8]. Using LFB, the small deformation modal response is computed in a local coordinate system at the center of mass within the rigid body [7]. Together with the superimposed modes, the body can undergo finite translations and rotations, i.e, rigid body motion.

An LFB is also formed using the ***CONTROL_IMPLICIT_MODES** keyword in combination with the previously mentioned implicit cards. It can be formed using eigenmodes alone or a combination of eigenmodes and constraint modes (and/or attachment modes). The LFB is introduced into the model using ***PART_MODES**. Contrary to the SE, the parts reduced shall remain in the model and be switched to rigid parts using the ***MAT_RIGID** keyword. Up until version R11.1, a model including an LFB could only be calculated using double precision. Note that, contrary to SE, LFB can be mass scaled since the elements still physically exist in the model.

3 Evaluation

In this work, SE based on Craig-Bampton and LFB based on Modal Truncation were evaluated. In order to do so, a structural frame was first considered. The frame is impacted by a sphere in order to introduce contact into the problem. Substructures were tied to the frame using tied contact and served as MOR candidates.

Based on the sensitivity of using LFB via constraint modes, and the fact that in the studied example it rendered a too small allowable time step, it was eliminated from the qualifying MOR methods. Not only that, but the time spent on preparing an LFB using constraint modes is large. The DoFs of the boundary nodes shall be accurately defined before reduction and upon running the ROM, the nodes shall be carefully switched to rigid. This is often hectic, error susceptible, and lasts long in large models such as vehicles. One wrong or missing node definition leads to several launching or simulation errors. In addition, models based on SE did not run using SMP LS-DYNA versions 10.2 and 11.1. In some cases, the model launched and then terminated due to the time step exceeding the allowable time step of the SE. On the other hand, running the same model using MPP LS-DYNA, using both versions, was successful and the time step was stable. The assessment was thus performed using MPP LS-DYNA.

3.1 Structural Frame with Small Displacements

3.1.1 Case 1

Several cases were considered to study the behaviour in small displacement and large displacement scenarios. In case 1, one substructure was attached to the frame using tied contact, on the other side of impact as shown in Fig. 1.

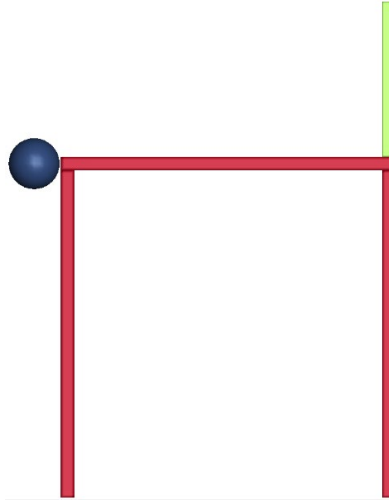


Fig.1: Fixed frame with 1 substructure impacted by a rigid ball

Both the frame and the substructure were modelled using accurate fully-integrated shell elements (`ELFORM=-16` on `*SECTION_SHELL`). These elements provide good accuracy in problems with large deformations/rotations over a single time step and combined with `IACC=1` on the `*CONTROL_ACCURACY` card, they ensure the correct transformation of stresses and avoid the formation of spurious strains, i.e., hourglass [8]. The frame is composed of 7550 elements while the substructure of 4880. The dimensions of the first are double those of the second except for the thickness which is the same. All the frame's bottom support nodes were fully constrained. On the other hand, the impacting sphere was modelled using 384 rigid solid elements. The sphere impacts the frame at a speed of 100 Km/hr (≈ 28 m/s) and the Automatic Single Surface contact was used for handling the contact algorithm. A simulation time of 60 ms was considered. The models were ran using MPP LS-DYNA R11.1 with double precision on an HPC, a property of SCALE GmbH. The HPC has the properties shown in Tab. 1. Each model (full, SE, LFB) and its variants (15 EM, 30 EM) was ran 3 times. This is in order to ensure that there is time consistency and the methods' efficiency can be safely evaluated.

| Feature | Description |
|----------------------|-------------------------------------|
| Model | Intel® Xeon® CPU E5-2660 v3 @2.6GHz |
| Number of Processors | 40 |
| Memory (MB) | 65868 |

Table 1: Properties of the HPC used

The time performance of SE and LFB for case 1 can be seen in Tab. 2. Note that the “mean” refers to the arithmetic mean and “Red.” refers to reduction. It can be seen that, using 15 EM, the SE approach managed to achieve a 38% average time reduction while the LFB approach a 28%. With the increase of EM from 15 to 30, the performance of SE dropped by 1% while that of LFB by 10%.

(a) 15 Eigenmodes

| | Full | | | | SE 15 | | | | LFB 15 | | | |
|----------|------|-----|-----|------|-------|-----|-----|------|--------|-----|-----|------|
| Run | 1 | 2 | 3 | Mean | 1 | 2 | 3 | Mean | 1 | 2 | 3 | Mean |
| Time [s] | 896 | 907 | 905 | 903 | 556 | 553 | 560 | 556 | 670 | 643 | 645 | 653 |
| Red. [%] | | | | | 38 | 39 | 38 | 38 | 26 | 29 | 29 | 28 |

(b) 30 Eigenmodes

| | Full | | | | SE 30 | | | | LFB 30 | | | |
|----------|------|-----|-----|------|-------|-----|-----|------|--------|-----|-----|------|
| Run | 1 | 2 | 3 | Mean | 1 | 2 | 3 | Mean | 1 | 2 | 3 | Mean |
| Time [s] | 896 | 907 | 905 | 903 | 572 | 566 | 580 | 573 | 741 | 742 | 734 | 739 |
| Red. [%] | | | | | 37 | 37 | 36 | 37 | 18 | 18 | 19 | 18 |

Table 2: Time performance of case 1

In order to further understand the reason behind such a large difference in performance, the time breakdown of the analysis was assessed. This breakdown can be obtained from the `message` or `d3hsp` files. The main processes that consume time are element processing (EP) and contact algorithm (CA). Accordingly, these two main processes were examined, in addition to rigid body (RB) handling. Recalling that LFB is based on switching reduced parts to rigid, observing the time behaviour of rigid bodies makes sense. The comparison is provided in Tab. 3.

| (a) 15 Eigenmodes | | | | | | | | | | | | |
|-------------------|------|-----|-----|------|-------|-----|-----|------|--------|-----|-----|------|
| | Full | | | | SE 15 | | | | LFB 15 | | | |
| Run | 1 | 2 | 3 | Mean | 1 | 2 | 3 | Mean | 1 | 2 | 3 | Mean |
| EP [s] | 771 | 780 | 779 | 776 | 463 | 460 | 465 | 463 | 495 | 474 | 474 | 481 |
| CA [s] | 81 | 82 | 81 | 81 | 47 | 47 | 47 | 47 | 64 | 63 | 63 | 63 |
| RB [s] | 3 | 3 | 3 | 3 | 14 | 14 | 15 | 14 | 66 | 63 | 63 | 64 |

| (b) 30 Eigenmodes | | | | | | | | | | | | |
|-------------------|------|-----|-----|------|-------|-----|-----|------|--------|-----|-----|------|
| | Full | | | | SE 30 | | | | LFB 30 | | | |
| Run | 1 | 2 | 3 | Mean | 1 | 2 | 3 | Mean | 1 | 2 | 3 | Mean |
| EP [s] | 771 | 780 | 779 | 776 | 474 | 469 | 483 | 475 | 490 | 490 | 486 | 488 |
| CA [s] | 81 | 82 | 81 | 81 | 48 | 48 | 48 | 48 | 66 | 67 | 65 | 66 |
| RB [s] | 3 | 3 | 3 | 3 | 16 | 16 | 16 | 16 | 137 | 137 | 136 | 137 |

Table 3: Time breakdown of case 1

It is noticed that, when it comes to EP, both SE and LFB had a similar performance providing 40% and 38% average time reduction with 15 EM respectively and 39% and 37% with 30 EM respectively. On the other hand, regarding CA, a large difference between SE and LFB is observed. SE provided 42% and 41% reduction with 15 EM and 30 EM respectively, while LFB only 22% and 19%. Furthermore, both methods increased the time of RB handling, however the gap between the two was also significant. SE increased the time by 365% and 420% with 15 and 30 EM respectively, while LFB by 2000% and 4388%! Of course, such a large percentage is because the original RB handling time is only 3 seconds in the full model. Therefore, the share of the RB handling time from the total run time is assessed. In the full model it was only 0.34%, using SE it became 2.54% and 2.76% with 15 and 30 EM respectively, while using LFB, it jumped to 9.8% and 18.49% with 15 and 30 EM respectively. In addition, one can notice that RB handling lies behind the reduced reduction capabilities of LFB in comparison to SE and as the number of EV increases. One can notice that EP and CA almost stayed the same as the EV increased from 15 to 30 while RB more than doubled (114% increase).

Time performance alone is not sufficient to decide whether a method is efficient or not. The accuracy of the calculations was evaluated based on several physical quantities: total energy, internal energy, kinetic energy, resultant displacement, and resultant speed. The last two were assessed at the top right corner of the main frame (node 100000 in Fig. 2). A Butterworth filter with a cut-off frequency of 60Hz was used to filter the energies and speed.



Fig.2: Evaluation node for resultant nodal displacement and velocity

Several observations can be made from the comparisons. Observing the internal energy plots (see Fig. 3), one can notice that in the very early stage of impact (up to 6 ms) the curves are all aligning. However, as the time progresses, all methods deviate from the FOM yet maintaining a similar curve shape. The error at the second peak is around 150 KN-mm which is around 12%.

Regarding nodal resultant displacement, the methods tend to match the FOM at the very early stage of impact as well (see Fig. 4). Ignoring the discrepancy at the first peak, one could even say that the methods align for around 19 ms. The plots also have a similar shape to that of the FOM, with the SE

being more similar. Both methods tend to overestimate the behaviour; the error at the second peak is around 44% for LFB and 34% for SE. Similar observations were made regarding nodal velocity. Yet, the accuracy is influenced by the choice of the extracted EM and their number.

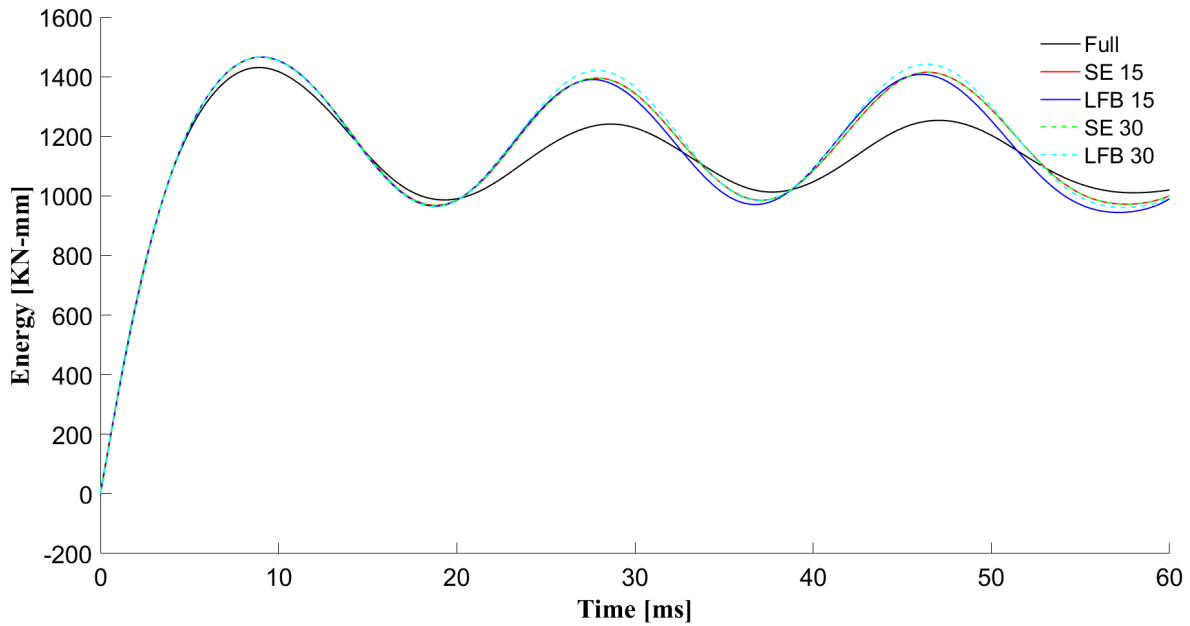


Fig.3: Internal energy evaluation for case 1

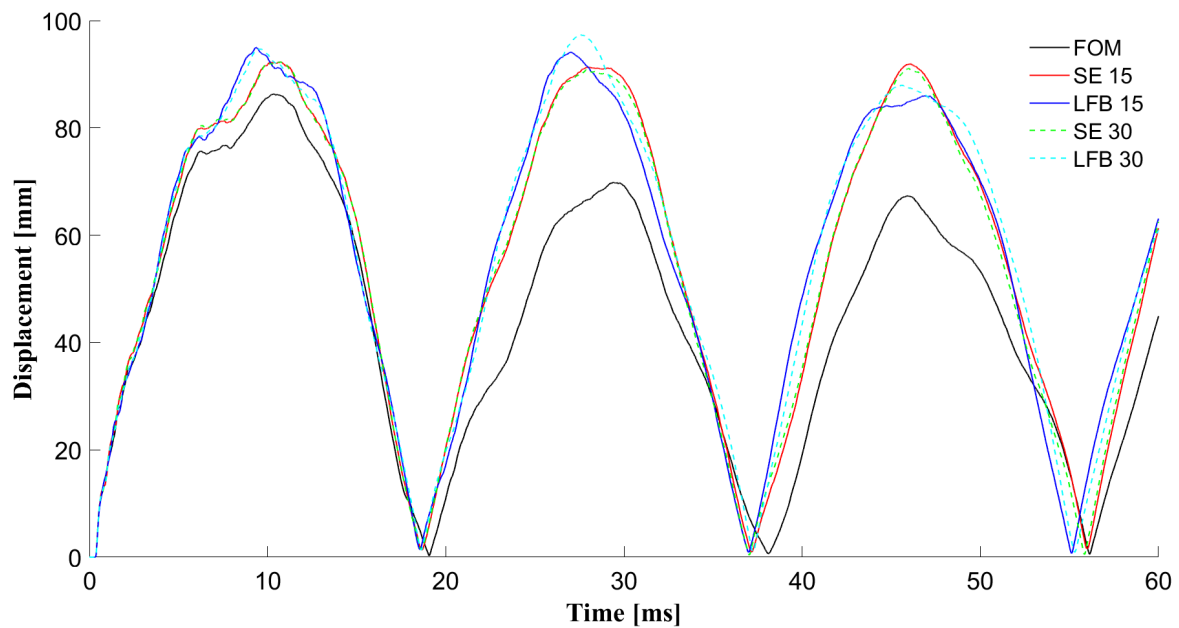


Fig.4: Nodal resultant displacement evaluation for case 1

3.1.2 Case 2

Case 2 was based on two substructures attached to the frame at different locations and lacking any internal interaction (see Fig. 7). Two cases are distinguished; in the first, case 2a, each substructure is reduced alone while in the other, case 2b, both are reduced together. The time performance of case 2a can be seen in Tab. 4 and that of 2b in Tab. 5. Note that, for case 2a, 15 or 30 EM indicate that each substructure was reduced using 15 or 30 EM; while for case 2b, it indicates that both together were reduced using 15 or 30 EM. It is noticed that SE achieved around 53% time-reduction in all cases. On the other hand, LFB achieved a good reduction when the two parts were reduced together. With 15 EM, it provided a time performance close to that of SE with an average of 46%.

In general, the better performance with regards to time in case 2 could be related to the size of the reduced part of the model in comparison to the size of the full model. In case 1, the reduced part accounted for 14% of the total mass (also volume) while in case 2 it accounted for 24%.

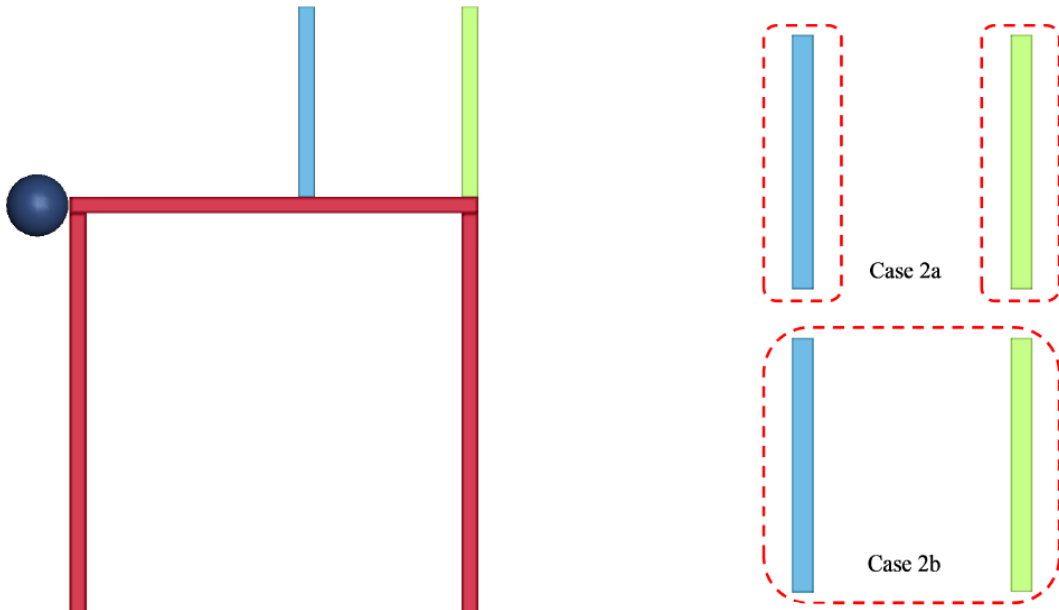


Fig.5: Case 2 of the structural frame. The red dotted lines enclose the reduced system(s).

(a) 15 Eigenmodes

| Run | Full | | | | SE 15 | | | | LFB 15 | | | |
|----------|------|------|------|------|-------|-----|-----|------|--------|-----|-----|------|
| | 1 | 2 | 3 | Mean | 1 | 2 | 3 | Mean | 1 | 2 | 3 | Mean |
| Time [s] | 1257 | 1260 | 1266 | 1261 | 587 | 585 | 586 | 586 | 754 | 769 | 753 | 759 |
| Red. [%] | | | | | 53 | 54 | 54 | 54 | 40 | 39 | 40 | 40 |

(b) 30 Eigenmodes

| Run | Full | | | | SE 30 | | | | LFB 30 | | | |
|----------|------|------|------|------|-------|-----|-----|------|--------|-----|-----|------|
| | 1 | 2 | 3 | Mean | 1 | 2 | 3 | Mean | 1 | 2 | 3 | Mean |
| Time [s] | 1257 | 1260 | 1266 | 1261 | 600 | 598 | 597 | 598 | 926 | 932 | 930 | 929 |
| Red. [%] | | | | | 52 | 53 | 53 | 53 | 27 | 26 | 26 | 26 |

Table 4: Time performance of case 2a

(a) 15 Eigenmodes

| Run | Full | | | | SE 15 | | | | LFB 15 | | | |
|----------|------|------|------|------|-------|-----|-----|------|--------|-----|-----|------|
| | 1 | 2 | 3 | Mean | 1 | 2 | 3 | Mean | 1 | 2 | 3 | Mean |
| Time [s] | 1257 | 1260 | 1266 | 1261 | 590 | 595 | 591 | 592 | 690 | 684 | 681 | 685 |
| Red. [%] | | | | | 53 | 53 | 53 | 53 | 45 | 46 | 46 | 46 |

(b) 30 Eigenmodes

| Run | Full | | | | SE 30 | | | | LFB 30 | | | |
|----------|------|------|------|------|-------|-----|-----|------|--------|-----|-----|------|
| | 1 | 2 | 3 | Mean | 1 | 2 | 3 | Mean | 1 | 2 | 3 | Mean |
| Time [s] | 1257 | 1260 | 1266 | 1261 | 594 | 598 | 596 | 596 | 872 | 870 | 868 | 870 |
| Red. [%] | | | | | 52 | 53 | 53 | 53 | 31 | 31 | 31 | 31 |

Table 5: Time performance of case 2b

Note that, when the two substructures are reduced each alone, the model has two SEs/LFBs and when reduced together, only one. Similar to case 1, increasing the number of EM didn't influence the reduction of SE, while that of LFB was affected by around 15%.

To better understand the reasons behind such observations, the time breakdown was assessed. The breakdowns can be seen in Tab. 6 and Tab. 7. Similar to case 1, both methods reduced EP, significantly and similarly. The reduction was almost the same, whether the two substructures were reduced together or separately and whether 15 or 30 EM were used. Using SE the reduction was about 56%, whereas using LFB it was about 54%. On the other hand, similar to case 1 as well, SE performed much better when it came to CA. The reduction was also almost not affected by the sub-cases and number of EM,

with SE achieving reductions around 53% while LFB around 28%, almost half that of SE. Once again, RB handling turned out to be the main reason behind such a large difference in performance between SE and LFB. The original share of RB in the FOM was 0.3%, using SE it was about 3.5% in all cases, while using LFB it was highly case-dependent. When the two substructures were reduced each alone, the RB share was about 16% with 15 EM and 30% with 30 EM. When the two substructures were reduced together, this share dropped to about 9% and 26% with 15 and 30 EM respectively.

(a) 15 Eigenmodes

| Run | Full | | | | SE 15 | | | | LFB 15 | | | |
|--------|------|------|------|------|-------|-----|-----|------|--------|-----|-----|------|
| | 1 | 2 | 3 | Mean | 1 | 2 | 3 | Mean | 1 | 2 | 3 | Mean |
| EP [s] | 1089 | 1088 | 1095 | 1090 | 481 | 477 | 476 | 478 | 493 | 505 | 491 | 496 |
| CA [s] | 112 | 113 | 113 | 113 | 52 | 54 | 52 | 52 | 80 | 80 | 81 | 80 |
| RB [s] | 3 | 3 | 3 | 3 | 19 | 20 | 21 | 20 | 124 | 127 | 124 | 125 |

(b) 30 Eigenmodes

| Run | Full | | | | SE 30 | | | | LFB 30 | | | |
|--------|------|------|------|------|-------|-----|-----|------|--------|-----|-----|------|
| | 1 | 2 | 3 | Mean | 1 | 2 | 3 | Mean | 1 | 2 | 3 | Mean |
| EP [s] | 1089 | 1088 | 1095 | 1090 | 485 | 484 | 485 | 484 | 503 | 504 | 511 | 506 |
| CA [s] | 112 | 113 | 113 | 113 | 54 | 53 | 54 | 54 | 84 | 82 | 82 | 83 |
| RB [s] | 3 | 3 | 3 | 3 | 23 | 23 | 22 | 22 | 277 | 285 | 274 | 279 |

Table 6: Time breakdown of case 2a

(a) 15 Eigenmodes

| Run | Full | | | | SE 15 | | | | LFB 15 | | | |
|--------|------|------|------|------|-------|-----|-----|------|--------|-----|-----|------|
| | 1 | 2 | 3 | Mean | 1 | 2 | 3 | Mean | 1 | 2 | 3 | Mean |
| EP [s] | 1089 | 1088 | 1095 | 1090 | 478 | 482 | 479 | 480 | 496 | 487 | 485 | 489 |
| CA [s] | 112 | 113 | 113 | 113 | 53 | 53 | 52 | 52 | 79 | 79 | 78 | 79 |
| RB [s] | 3 | 3 | 3 | 3 | 20 | 19 | 20 | 19 | 61 | 64 | 64 | 63 |

(b) 30 Eigenmodes

| Run | Full | | | | SE 30 | | | | LFB 30 | | | |
|--------|------|------|------|------|-------|-----|-----|------|--------|-----|-----|------|
| | 1 | 2 | 3 | Mean | 1 | 2 | 3 | Mean | 1 | 2 | 3 | Mean |
| EP [s] | 1089 | 1088 | 1095 | 1090 | 485 | 484 | 485 | 484 | 507 | 502 | 502 | 504 |
| CA [s] | 112 | 113 | 113 | 113 | 54 | 53 | 54 | 54 | 82 | 82 | 82 | 82 |
| RB [s] | 3 | 3 | 3 | 3 | 23 | 23 | 22 | 22 | 223 | 224 | 221 | 223 |

Table 7: Time breakdown of case 2b

Regarding accuracy, similar comments to those of case 1 can be made. The displacement plots are shown in Fig. 6 and 7.

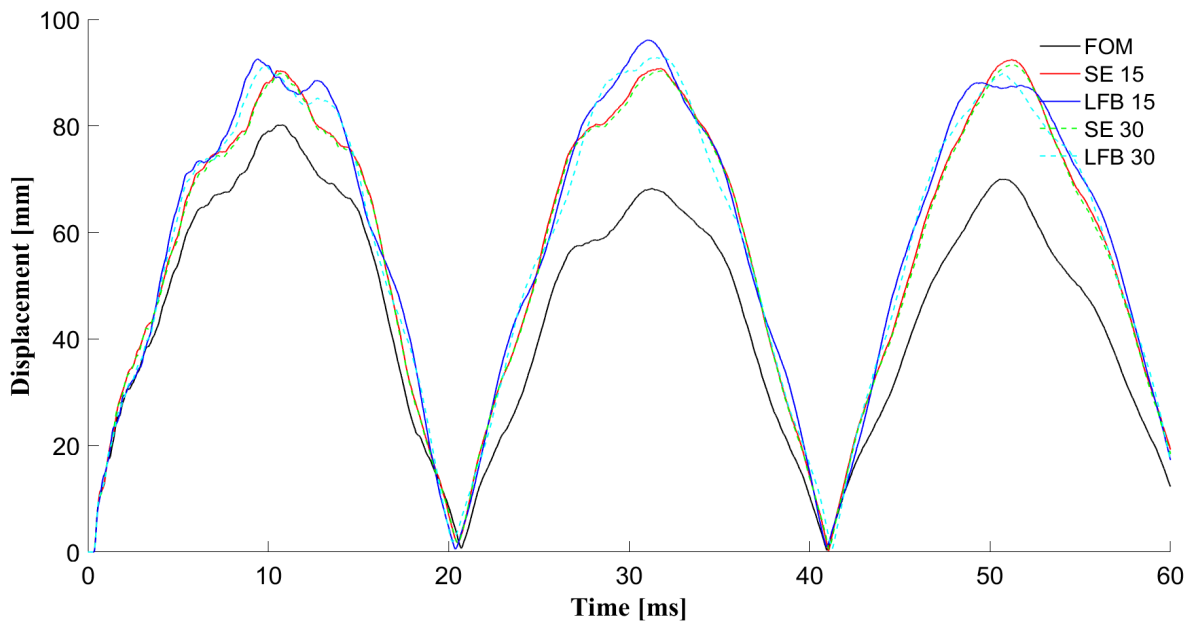


Fig.6: Nodal resultant displacement evaluation for case 2a

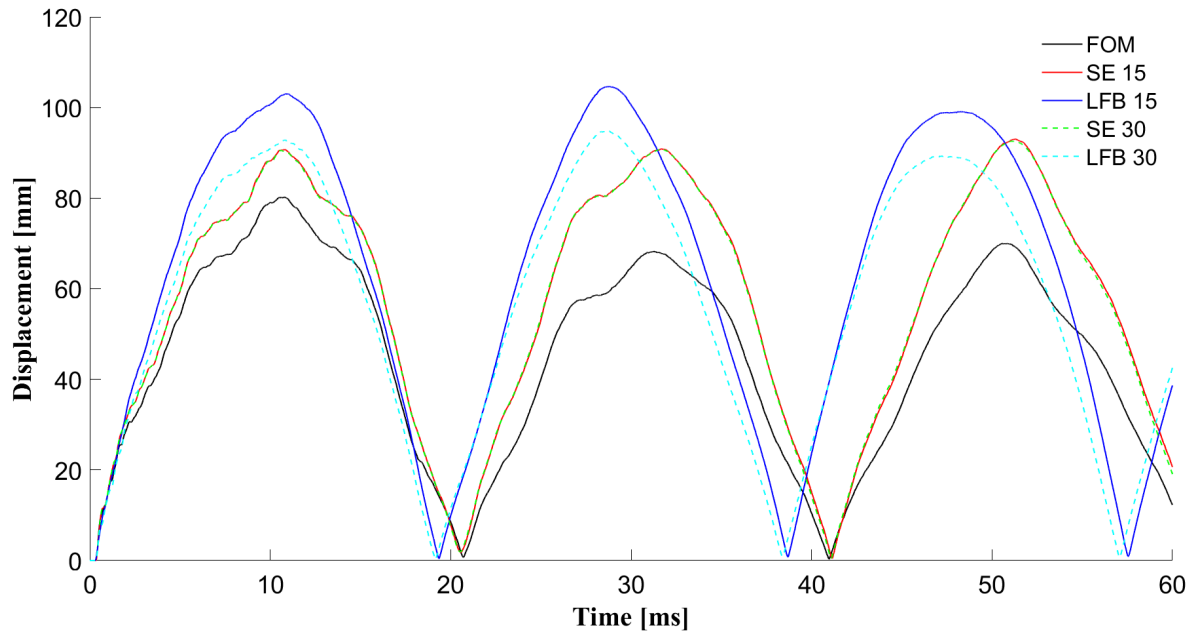


Fig.7: Nodal resultant displacement evaluation for case 2b

3.1.3 Case 3

In case 3, three substructures are attached to the frame (see Fig. 8). Two of them are directly attached to the frame, similar to case 2, while the third is attached to the other two using a tied contact at their top sides. In this manner, the three substructures are interactive, which means that the movement of one of them affects the movements of the other two, majorly the one(s) in direct contact with it. Based on the previous conclusion that having one reduced system is more efficient, the three substructures were only reduced together.

The time performance can be seen in Tab. 8. SE achieved a 63% reduction with both 15 and 30 EM. On the other hand, LFB provided a 46% reduction with 15 EM and a 29% one with 30 EM. The increase in the reduction of SE (53% in case 2b) is due to the increase in size of the reduced part from 24% to 33% of the total model size. However, despite this increase in size, LFB almost maintained the same reduction as in case 2b. With 15 EM the reduction stayed at 46% while with 30 EM it decreased slightly from 31% to 29%.

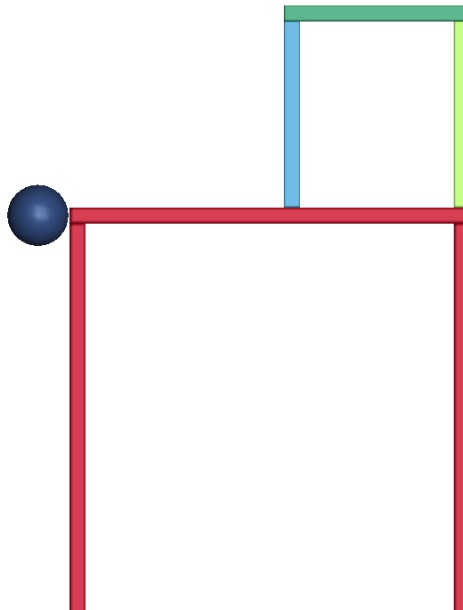


Fig.8: Case 3 of the structural frame

| (a) 15 Eigenmodes | | | | | | | | | | | | |
|-------------------|------|------|------|------|-------|-----|-----|------|--------|-----|-----|------|
| | Full | | | | SE 15 | | | | LFB 15 | | | |
| Run | 1 | 2 | 3 | Mean | 1 | 2 | 3 | Mean | 1 | 2 | 3 | Mean |
| Time [s] | 1787 | 1768 | 1756 | 1770 | 653 | 648 | 651 | 651 | 971 | 957 | 957 | 962 |
| Red. [%] | | | | | 63 | 63 | 63 | 63 | 45 | 46 | 46 | 46 |

| (b) 30 Eigenmodes | | | | | | | | | | | | |
|-------------------|------|------|------|------|-------|-----|-----|------|--------|------|------|------|
| | Full | | | | SE 30 | | | | LFB 30 | | | |
| Run | 1 | 2 | 3 | Mean | 1 | 2 | 3 | Mean | 1 | 2 | 3 | Mean |
| Time [s] | 1787 | 1768 | 1756 | 1770 | 646 | 646 | 646 | 646 | 1267 | 1250 | 1257 | 1258 |
| Red. [%] | | | | | 64 | 64 | 64 | 64 | 28 | 29 | 29 | 29 |

Table 8: Time performance of case 2a (in seconds)

The time breakdown (see Tab. 9) reflects again, that EP was reduced, significantly and similarly, by both methods and the reduction was not affected by the increase in EM. SE achieved a 67% reduction while LFB a 65% one. CA was also significantly reduced and was not affected by the increase in EM. A reduction of 56% was achieved using SE and 34% using LFB. Last but not least, similar to the previous cases, RB handling increased drastically. In the FOM it accounted for 0.2%, using SE for 4%, while using LFB with 15 EM it was 25% while with 30 EM it jumped to 42%.

| (a) 15 Eigenmodes | | | | | | | | | | | | |
|-------------------|------|------|------|------|-------|-----|-----|------|--------|-----|-----|------|
| | Full | | | | SE 15 | | | | LFB 15 | | | |
| Run | 1 | 2 | 3 | Mean | 1 | 2 | 3 | Mean | 1 | 2 | 3 | Mean |
| EP [s] | 1548 | 1516 | 1516 | 1527 | 505 | 501 | 504 | 503 | 536 | 527 | 524 | 529 |
| CA [s] | 164 | 164 | 164 | 164 | 72 | 72 | 72 | 72 | 110 | 109 | 109 | 109 |
| RB [s] | 4 | 4 | 4 | 4 | 26 | 26 | 26 | 26 | 238 | 236 | 238 | 237 |

| (b) 30 Eigenmodes | | | | | | | | | | | | |
|-------------------|------|------|------|------|-------|-----|-----|------|--------|-----|-----|------|
| | Full | | | | SE 30 | | | | LFB 30 | | | |
| Run | 1 | 2 | 3 | Mean | 1 | 2 | 3 | Mean | 1 | 2 | 3 | Mean |
| EP [s] | 1548 | 1516 | 1516 | 1527 | 502 | 502 | 499 | 501 | 534 | 527 | 527 | 529 |
| CA [s] | 164 | 164 | 164 | 164 | 71 | 71 | 71 | 71 | 110 | 109 | 110 | 110 |
| RB [s] | 4 | 4 | 4 | 4 | 26 | 25 | 26 | 25 | 535 | 526 | 533 | 531 |

Table 9: Time breakdown of case 2b

As for the accuracy of case 3, great improvements were observed. By examining the internal energy plot (see Fig. 9), it can be seen that both methods almost exactly replicate the FOM using only 15 EM. In fact, the plots of SE are exactly over those of the FOM while those of LFB introduce a minor phase shift. Similarly, examining the resultant displacement plots (see Fig. 10), it is evident that the SE matches the FOM exactly, be it with 15 or 30 EM, while the LFB slightly differs. However, this difference is not drastic or severe, especially in comparison to cases 1, 2a, and 2b.

The reason behind such a great improvement in accuracy, although the size of the reduced part increased and the number of EM is just 15, is believed to be related to the interactive nature of the reduced part. Since the three substructures are in contact, the 15 extracted EM actually induce vibrations in all three substructures at the same time. In other words, the extracted modes are those of a frame formed from the three substructures. On the other hand, when the two substructures were reduced, they had no contact and the extracted modes didn't excite both substructures at the same time due to discontinuity. In fact, upon inspecting the message file produced by LS-DYNA, it was found that with the two substructures, 12 out of the 15 EM were eliminated because they represented rigid-body-modes, while with the three interactive substructures, only 6 rigid-body-modes were eliminated.

Nevertheless, this alone doesn't justify the difference in accuracy, since upon increasing the EM from 15 to 30 in case 2, no improvements in accuracy were observed. This leaves us with the idea that the interactive nature and interconnectivity of the reduced part of the model has an influence on accuracy. The discontinuity is probably capable of strengthening the oscillatory behaviour of each substructure thus leading to the higher peaks in the plots of cases 1, 2a, and 2b.

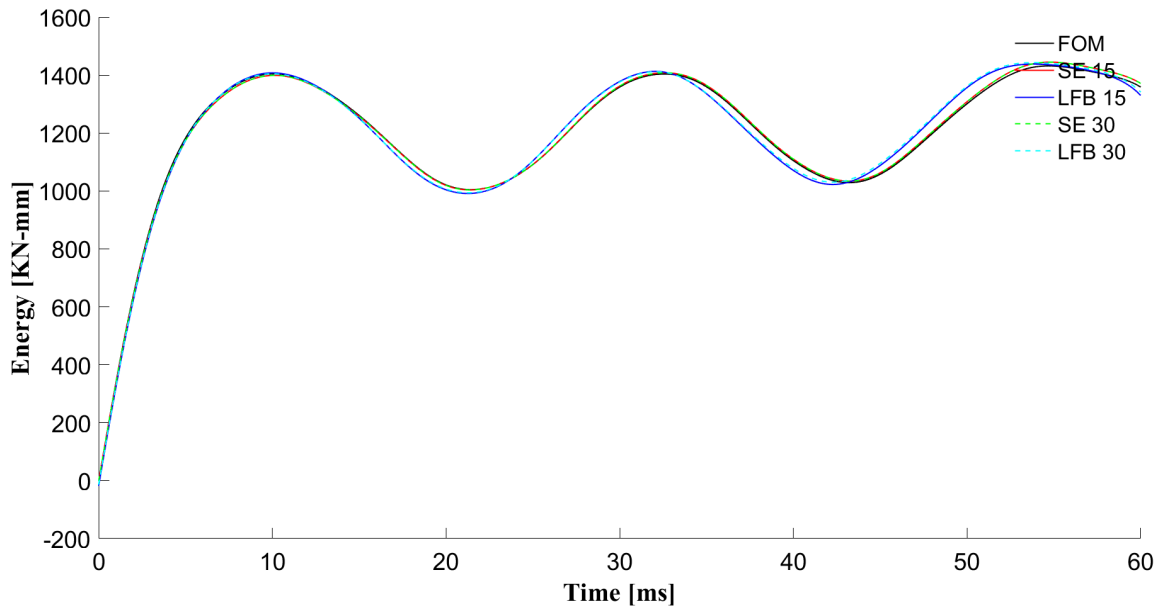


Fig.9: Internal energy evaluation for case 3

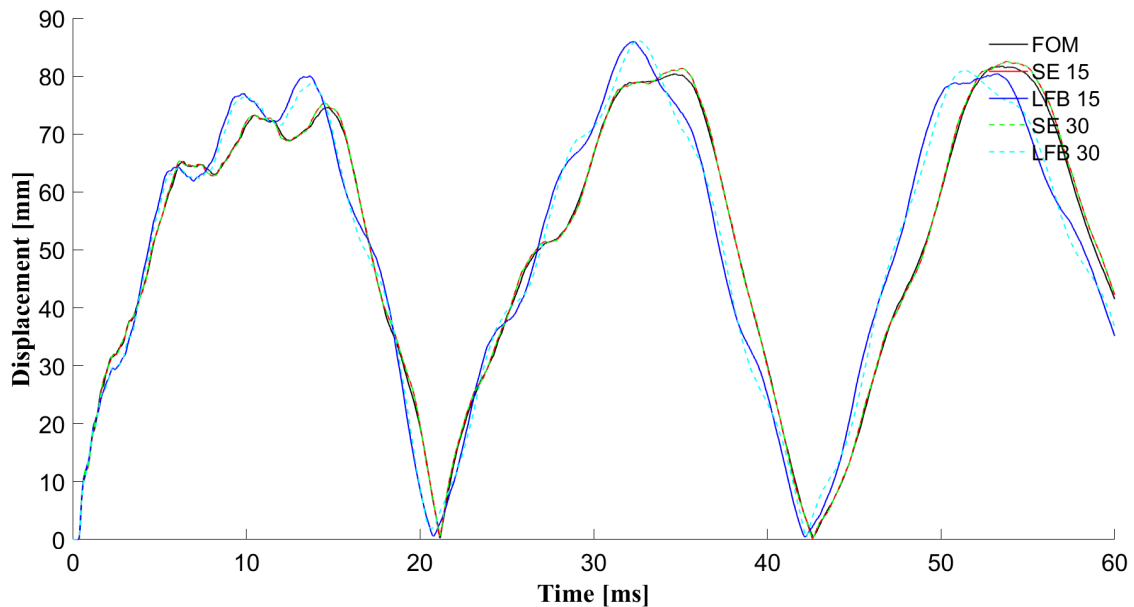


Fig.10: Nodal resultant displacement evaluation for case 3

In order not to limit the accuracy assessment to one node, the different deformation states across the simulation time were compared by overlaying the results of SE and LFB over those of the FOM. The final state, is presented here (see Fig. 11, 12, and 13). It is based on cases 1, 2a, and 3 using 15 EM. The full model is represented in red, the SE in green, and the LFB in dark blue. Note that since in the SE approach, the reduced part shall be deleted from the model, it is not evident in the state images.

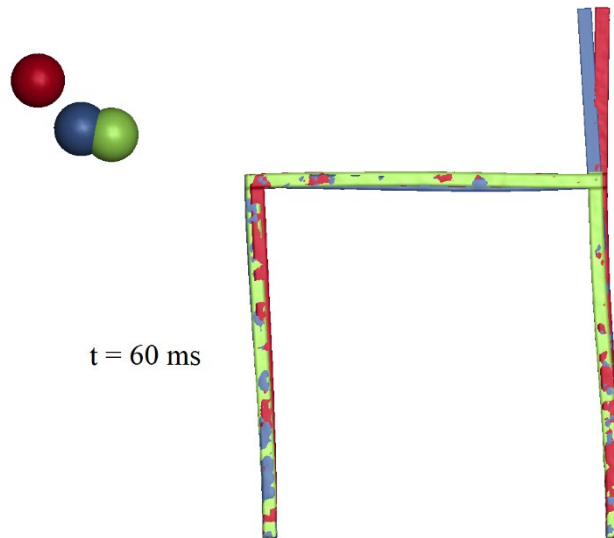


Fig.11: Final deformation state of case 1 using 15 EM

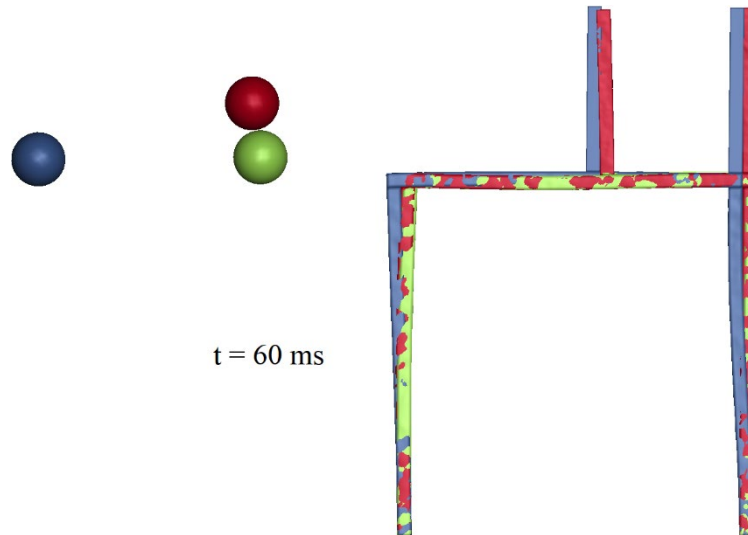


Fig.12: Final deformation state of case 2b using 15 EM

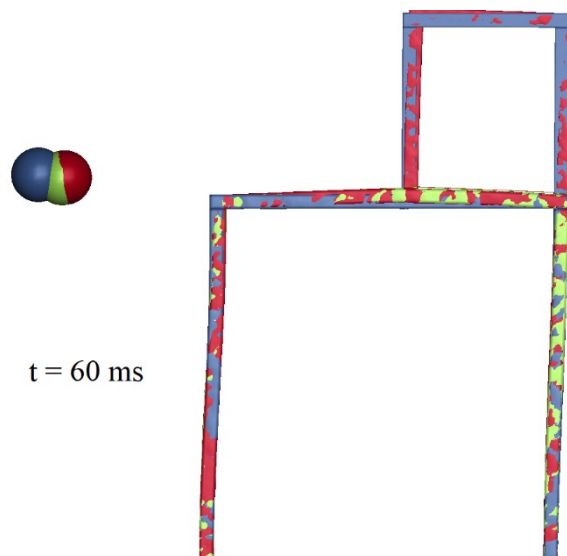


Fig.13: Final deformation state of case 3 using 15 EM

A summary of the time performance is provided in Fig. 14 and the following is summarized:

1. As the size of the reduced part increased, the total reduction increased. This is due to additional reductions in EP and CA, especially using SE.
2. Increasing the number of EM didn't influence the time performance of SE but influenced LFB majorly, due to the sharp increase in RB handling.
3. SE achieved higher reductions than LFB due to differences in CA and RB handling. With regards to EP, both achieved similar results.

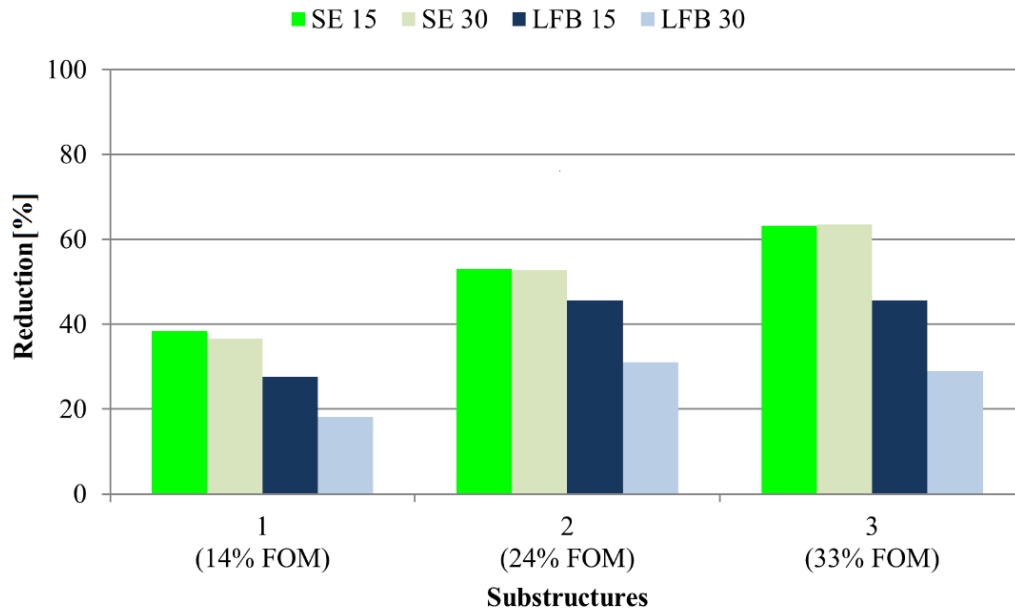


Fig. 14: Total reduction as a function of method, number of eigenmodes, and number of reduced substructures (size of reduced structure in %)

3.2 Structural Frame with Large Displacements

Since crash analysis revolves around large displacements and rigid body motion, it was decided to perform a pre-qualification test for the methods using a structural frame. The structural frame of case 3 was used to create case 4 by simply deleting the right vertical support of the frame (see Fig. 15). The deletion of the support reduces the stiffness of the frame, thus allowing it to displace more.

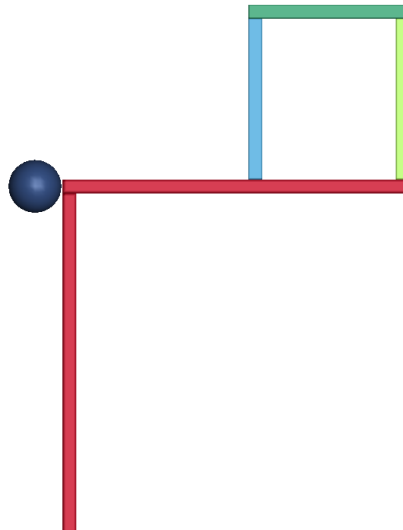


Fig. 15: Case 4 of the structural frame

The time performance (see Tab. 10) and breakdown (see Tab. 11) are also provided (only the mean is provided noting that the run time was also consistent). The increased reduction is attributed to the fact that the reduced part now represents 42% of the FOM size in comparison to 33% in case 3. Similar observations to those in section 3.1 regarding EP, CA, and RB can be made, thus are not discussed.

| | Full | SE 15 | LFB 15 | SE 30 | LFB 30 |
|----------|------|-------|--------|-------|--------|
| Time [s] | 1658 | 466 | 767 | 468 | 1077 |
| Red.[%] | | 72 | 54 | 72 | 35 |

Table 10: Time performance of case 4

| | Full | SE 15 | LFB 15 | SE 30 | LFB 30 |
|--------|------|-------|--------|-------|--------|
| EP [s] | 1405 | 345 | 361 | 348 | 367 |
| CA [s] | 175 | 53 | 91 | 53 | 92 |
| RB [s] | 4 | 26 | 239 | 26 | 538 |

Table 11: Time breakdown of case 4

The major observations are related to accuracy. The SE approach which perfectly aligned the FOM in case 3, shifted away from it in case 4, as the simulation time progressed (see Fig. 16 and Fig. 17). Yet, LFB provides a good performance.

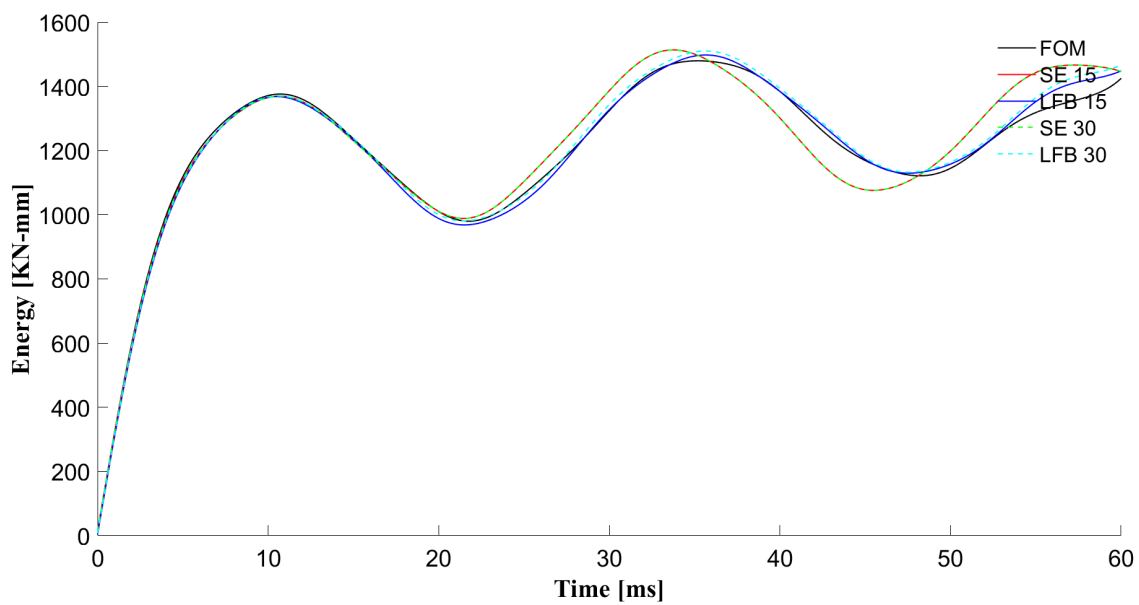


Fig.16: Internal energy evaluation for case 4

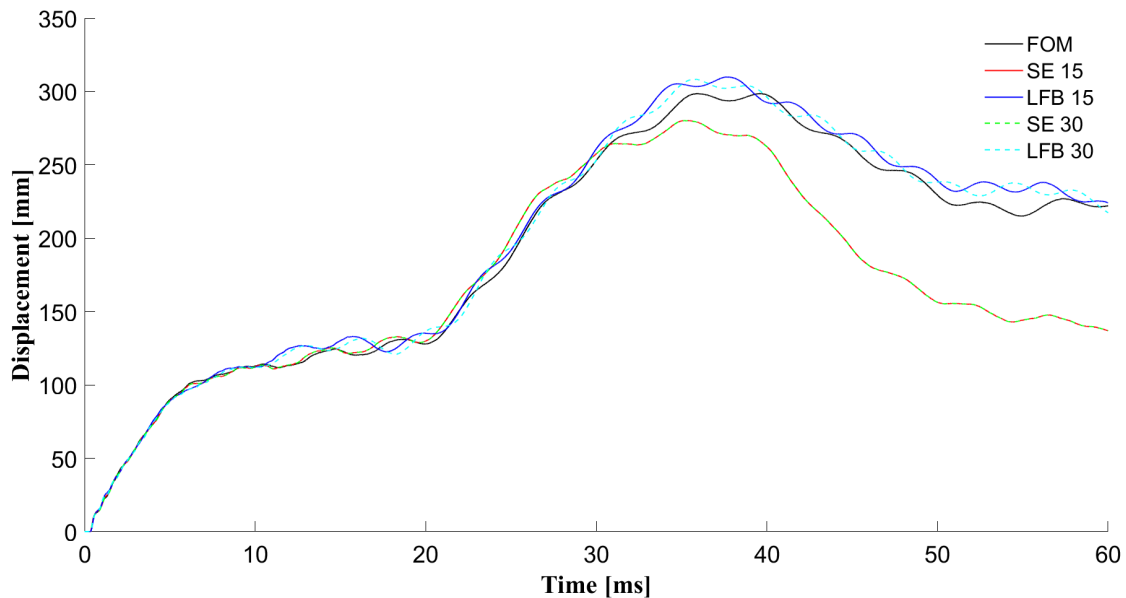


Fig.17: Nodal resultant displacement evaluation for case 4

4 Application in Crash Analysis

Following the success of LFB using EM in the structural frame cases 3 and 4, the assessment was then shifted to crash analysis. For this purpose, the Toyota Yaris 2010 FEM model, courtesy of [11], was used. There are different reasons behind this choice. First, it is available for free. Second, the numerical model was already validated by CCSA,[11], and thus its results are within the accuracy desired as per the international guidelines. Finally, the model is already implemented within the SDM software LoCo, which facilitates modifications, calculations, and assessments.

In addition to the previously explained LFB approach, another technique was also assessed for time reduction, but is not an MOR method. It is rather based on switching elements/parts to rigid without even reducing them. By doing so, the elements are not deformable and there exists no need to calculate their stresses and strains. The elements are bypassed in the EP and no storage is allocated for storing history variables; consequently, the rigid material type is very cost efficient [8]. Yet, since no history variables are stored, displacements and other quantities related to these parts can't be extracted, contrary to LFB.

There exist two possibilities to switch the parts to rigid. The first is by switching the material definition of the parts to a `*MAT_RIGID` definition, while the other is to use the `*DEFORMABLE_TO_RIGID` card. Using the latter, LS-DYNA switches the parts automatically at the start of the simulation. In general, the disadvantage of the first is that the parts are switched to rigid permanently. Using the second option, the parts can be switched back to deformable during the simulation. This can be achieved by using `*DEFORMABLE_TO_RIGID_AUTOMATIC` by which a certain criterion is defined to activate and/or deactivate the rigid behaviour. The disadvantage of the second option is that the choice of parts is restricted by the element type. For example, the Hughes-Liu formulation (`ELFORM=1` on `*SECTION_SHELL`) can't be used. In this work, the deformable to rigid (D2R) approach was used.

A side impact crash was performed for the study. However, the full vehicle model was not considered in order to simplify the model and limit the run time. Two model variants (see Fig. 18) were considered: variant 1 is composed of the body in white (BIW), hood, and hatch, while variant 2 is variant 1 plus the front crash management system and the four doors. The car body impacts a rigid pole barrier from the left side, at an angle of 90 degrees relative to it, and a speed of 50Km/hr. Two general reduction options were studied; in variant 1, the hood and the hatch were reduced, while in variant 2, all parts with the exception of the BIW and left side doors were reduced. The simulation time was 120 ms.

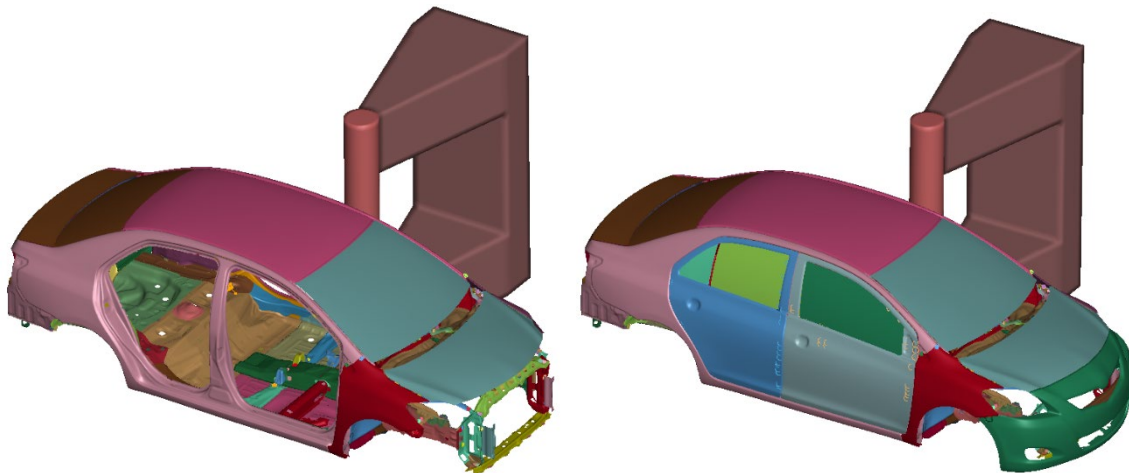


Fig. 18: Side impact crash model; variant 1 (left) variant 2 (right)

4.1 Time Consistency

One of the major challenges in this work was achieving consistent run times. Different simulation times were first attained when re-running a model, thus preventing the proper assessment of LFB and D2R. Fluctuations between the fastest and slowest run of a model ranged between 5% and 116%. Such time fluctuations were even encountered when a model was run alone on the cluster using all 40 CPUs, in which case the discrepancy was 38%.

In order to stabilize the run time, the default Recursive Coordinate Bisection (RCB) decomposition logic (see Fig. 19) was changed. Three different MPP decomposition strategies were tested independently: `CONTROL_MPP_DECOMPOSITION_CONTACT_DISTRIBUTE` which distributes the contact over all processors, `CONTROL_MPP_DECOMPOSITION_CHECK_SPEED` which modifies the decomposition depending on the processors' relative speed, and `CONTROL_MPP_DECOMPOSITION_AUTOMATIC` which decomposes the model parallel to velocity. For the studied example, the last decomposition keyword provided the best performance with only 0.7% time discrepancy.



Fig.19: Model decomposition using RCB (left) and `CONTROL_MPP_DECOMPOSITION_AUTO-MATIC` (right) over 8 CPUs. The rectangular highlights reflect the location of the reduced parts.

In addition, it was noticed that the cluster had an influence on the run-time of the simulations. The number of free CPUs and the number of simulations running in parallel influenced the run time. Accordingly, three computing environments were defined and studied: practical, weakly isolated, and strongly isolated. In a practical environment, a simulation is sent to the cluster without paying close attention to how many CPUs are currently active or how many runs are going on in parallel. In other words, the cluster is treated a Blackbox. In a weakly isolated environment, multiple runs of the same model can be running in parallel on the cluster without any other activity existing on the cluster. While in a strongly isolated environment, one and only one run of a model can be performed at a single time.

Running a model in a practical environment, in which the engineer doesn't pay close attention to what other activity is being performed by the HPC while performing the desired simulation, doesn't guarantee consistent times. Therefore, it doesn't guarantee that the reduction approach (LFB) and the rigid approach (D2R) would yield faster calculations. In addition, performing runs in a weakly isolated environment, where more than one run of the same model is performed simultaneously, provides different run times and reductions in comparison to a strongly isolated environment, where one and only one run is performed at a time on the HPC. The differences in the run time were more than 50% and those in reduction were more than 20%. A model which provided 27% reduction in a weakly isolated environment provided only 4% in a strongly isolated one.

4.2 Time Efficiency

4.2.1 Variant 1

Two cases were considered for this variant. In case 1, the hood and the hatch were reduced separately each with 15 EM. In case 2, they were reduced together using 30 EM. Since the two parts are not interactive, the extracted EM would not excite both substructures together, hence there would be a total of 12 rigid-body-motion EM. Therefore, choosing 30 EM would leave us with 18 useful ones, 9 per substructure. The time performance results can be seen in Tab. 12 and 13.

Similar to the structural frame example, reducing the substructures together enhanced MOR performance. The reduction increased from 12% to 26%. EP was reduced by 19% and CA by 15% when the reduction was done separately, and 30% and 31% respectively when the reduction was done together. RB handling again increased, by around 240%. Its share in the FOM was 0.9% while in LFB it jumped to 3.7%. A major observation is the good performance without a control card. The main reason, that could lie behind such a good performance, is that the load balance and communication are good

with 4 CPUs. This observation is thus related to scalability and the proper subdivision of the model over the processors.

(a) Time performance

| Run | Full | | | | LFB | | | |
|----------|--------|--------|--------|--------|--------|--------|--------|--------|
| | 1 | 2 | 3 | Mean | 1 | 2 | 3 | Mean |
| Time [s] | 44,547 | 44,551 | 44,483 | 44,172 | 39,020 | 38,974 | 39,066 | 39,020 |
| Red. [%] | | | | | 12 | 12 | 12 | 12 |

(b) Time breakdown

| Run | Full | | | | LFB | | | |
|--------|--------|--------|--------|--------|--------|--------|--------|--------|
| | 1 | 2 | 3 | Mean | 1 | 2 | 3 | Mean |
| EP [s] | 18,689 | 18,712 | 18,672 | 18,629 | 15,173 | 15,142 | 15,203 | 15,173 |
| CA [s] | 17,187 | 17,158 | 17,169 | 17,028 | 14,444 | 14,439 | 14,449 | 14,444 |
| RB [s] | 433 | 430 | 424 | 423 | 1,427 | 1,429 | 1,426 | 1,427 |

Table 12: LFB performance of variant 1 case 1

(a) Time performance

| Run | Full | | | | LFB | | | |
|----------|--------|--------|--------|--------|--------|--------|--------|--------|
| | 1 | 2 | 3 | Mean | 1 | 2 | 3 | Mean |
| Time [s] | 44,547 | 44,551 | 44,483 | 44,172 | 32,632 | 32,646 | 32,682 | 32,653 |
| Red. [%] | | | | | 26 | 26 | 26 | 26 |

(b) Time breakdown

| Run | Full | | | | LFB | | | |
|--------|--------|--------|--------|--------|--------|--------|--------|--------|
| | 1 | 2 | 3 | Mean | 1 | 2 | 3 | Mean |
| EP [s] | 18,689 | 18,712 | 18,672 | 18,629 | 13,082 | 13,081 | 13,135 | 13,099 |
| CA [s] | 17,187 | 17,158 | 17,169 | 17,028 | 11,813 | 11,839 | 11,782 | 11,811 |
| RB [s] | 433 | 430 | 424 | 423 | 1,523 | 1,524 | 1,520 | 1,522 |

Table 13: LFB performance of variant 1 case 2

4.2.2 Variant 2

Five substructures -hood, hatch, crash management system, and the two right-side doors- were reduced together. The two cases, FOM and LFB, were first ran using 4 CPUs, with and without the MPP control card. Table 14 shows the mean value of runs performed for each case along with the discrepancy and LFB time reduction (based on the mean value). With the control card, consistent times were achieved reflected by the low discrepancy ($\leq 1\%$) but the LFB performance was negative (-9%). On the other hand, in the absence of the card, the discrepancy was slightly higher (2-3%) but LFB had a positive performance (14%). Similar to variant 1, this can be the result of good load balance and communication using RCB decomposition over 4 CPUs, thus requiring no decomposition control.

(a) Time performance

| | With MPP Control | | Without MPP Control | |
|-----------|------------------|--------|---------------------|--------|
| | Full | LFB | Full | LFB |
| Time [s] | 59,027 | 64,453 | 56,508 | 49,020 |
| Red. [%] | - | -9 | - | 14 |
| Disc. [%] | 1 | 0.6 | 3 | 2 |

(b) Time breakdown

| | With MPP Control | | Without MPP Control | |
|-----------|------------------|--------|---------------------|--------|
| | Full | LFB | Full | LFB |
| Time [s] | 24,578 | 19,097 | 22,937 | 15,391 |
| Red. [%] | 23,489 | 23,332 | 21,436 | 14,795 |
| Disc. [%] | 564 | 9,382 | 476 | 7,586 |

Table 14: MPP control card influence on LFB performance using 4 CPUs

The influence of the MPP control card was also studied on a different number of processors (see Tab. 15) The major role this card plays in achieving consistent run-time when more than 4 CPUs are used is evident. It was also evident that as the number of CPUs increased, the performance of LFB and D2R changed drastically (see Tab. 16). LFB provided positive time reduction using 8 CPUs, contrary to when 4 or 12 CPUs were used. In addition, the performance of D2R dropped significantly when 12 CPUs were used.

| (a) 8 CPUs | | | | | | |
|-------------|--------|--------|--------|--------|--------|-----------|
| | Run 1 | Run 2 | Run 3 | Run 4 | Mean | Disc. [%] |
| without | 29,450 | 29,921 | 30,943 | 30,910 | 30,306 | 2.8 |
| with | 33,192 | 33,113 | 33,073 | 33,008 | 33,097 | 0.2 |
| (b) 16 CPUs | | | | | | |
| | Run 1 | Run 2 | Run 3 | Run 4 | Mean | Disc. [%] |
| without | 18,109 | 19,779 | 13,891 | 13,861 | 16,410 | 43 |
| with | 13,070 | 13,122 | 13,097 | 13,082 | 13,093 | 0.4 |

Table 15: Influence of CONTROL_MPP_DECOMPOSITION_AUTOMATIC on time consistency of model variant 2 using 8 and 16 processors (with and without MPP control).

By examining the time breakdown, a deeper understanding of what is happening can be achieved. LFB didn't reduce the CA at all using 4 and 12 CPUs, however using 8 CPUs it reduced it by 27%. D2R reduced the CA by 47% and 39% using 4 and 8 CPUs respectively and only 5% using 12 CPUs! Regarding EP, both methods reduced it similarly using 8 (35%) and 12 (23%) CPUs. However, D2R was able to reduce it by 44% using 4 CPUs while LFB only 22%. RB handling significantly increased using LFB, as usual, while using D2R it remained insignificant, explaining the reason why D2R overcame LFB with regards to time performance.

All of this can be related to scalability of the model and its decomposition, achieved here via the CONTROL_MPP_DECOMPOSITION_AUTOMATIC. One can deduce that depending on the number of CPUs, a particular decomposition logic is not guaranteed to provide the same performance.

| (a) Time performance | | | | | | | | | |
|----------------------|----------|----------|-----------|----------|----------|-----------|----------|----------|-----------|
| | 4 CPUs | | | 8 CPUs | | | 12 CPUs | | |
| | Time [s] | Red. [%] | Disc. [%] | Time [s] | Red. [%] | Disc. [%] | Time [s] | Red. [%] | Disc. [%] |
| Full | 59,027 | - | 1 | 33,556 | - | 1 | 16,346 | - | 3 |
| LFB 40 | 64,453 | -9 | 0.6 | 29,391 | 12 | 0.4 | 17,562 | -7 | 3 |
| D2R | 33,291 | 44 | 3 | 21,734 | 35 | 0.2 | 14,955 | 9 | 1 |

| (b) Time breakdown (in seconds) | | | | | | | | | |
|---------------------------------|--------|--------|-------|--------|--------|-------|---------|-------|-------|
| | 4 CPUs | | | 8 CPUs | | | 12 CPUs | | |
| | EP | CA | RB | EP | CA | RB | EP | CA | RB |
| Full | 24,578 | 23,489 | 564 | 12,056 | 13,060 | 602 | 6,228 | 5,553 | 433 |
| LFB 40 | 19,097 | 23,332 | 9,382 | 7,844 | 9,519 | 4,012 | 4,819 | 5,507 | 2,235 |
| D2R | 13,884 | 12,526 | 541 | 7,705 | 7,952 | 562 | 4,862 | 5,287 | 508 |

Table 16: Influence of the number of CPUs on performance using the control card

4.3 Accuracy

The accuracy of model variant 2 was studied using two ways: data history and state overlaying. Using data history, different nodes of the vehicle were assessed with regards to the resultant displacement. These points belong to the reduced and non-reduced parts. Some of these points are shown in Fig. 20. The average resultant displacements of the BIW can be seen in Fig. 21. It is evident that both methods underestimated the displacements, keeping in mind that for LFB only 40 EM were used.

In addition, the state at 80 ms, the time at which the car collision phase ends and the car starts to rebound back, is compared (see Fig. 22). The FOM is represented in black, LFB in blue, and D2R in red. The discrepancy in the behaviour of both LFB and D2R is evident.

5 Integration in SDM workflows

Another challenge of using MOR is its integration into simulation. Depending on the method (SE, LFB, etc.) used, a model must be modified in a particular manner in order to properly incorporate reduced model parts. It is essential that no redundancies or contradictions exist in the model, such as having a part in both, reduced and full order representation. These could cause a series of errors that would end up increasing the working time rather than reducing it, and complicating an engineer's life rather than easing it. To overcome such a challenge, a simulation data management (SDM) system can be used to automate the integration process. Using an SDM, the engineer can easily manipulate a model, deciding which parts (sub-models) are to be represented using an MOR-variant and which parts are to be retained in full order representation.

In this work, the SDM system "SCALE.sdm (LoCo)" was used to set up the whole process, submit runs to the HPC, and perform all the required automated post-processing. The reduction of the sub-models was done locally. The files including the reduced representation of the sub-models were saved and uploaded to LoCo. Within LoCo different possible combinations of reduced and unreduced parts of the model (frame and Yaris) were defined and even parameterized. By simply selecting a predefined model combination and modifying parameters, new studies were done at ease. The comparison of the outcome of the different studies was also easily done due to the interface of LoCo and CAVIT. Not only that, but using LoCo helped maintain and keep track of all the studied runs and changes done,

Another advantage of SDM, which was not implemented in this work, but would rather be advantageous, is to use the software itself to perform the reduction. The engineer would define the parts of the model which shall be reduced and provide the necessary reduction parameters. A reduction main file with the necessary cards and parameters would serve as a template for all reduction processes of a certain type (LFB, SE...). This main file would call the keyword file of the part(s) to be reduced via the include keyword. The reduction is then locally or over the cluster performed, and the file would be saved within the SDM software. Following that, the parts that were reduced would be either switched to rigid in the LFB approach or eliminated from the assembly process in the SE approach. Using LFB, this would require changing the material card definition, while using SE this would require removing the include command for the reduced parts. Such a process can be automated using a script that handles all of these processes and creates the desired model setting within the SDM software environment. Furthermore, an automated post-processing can be used to identify areas (sub-models) exhibiting linear behavior. These sub-models would then be candidates for linear MOR. This would require analyzing the output data, searching for patterns of linearity. There are different possibilities to do so, however, these were not investigated or implemented in this work; thus, they serve as topics for future investigation.

6 Summary

For small displacement problems, it was noticed that the SE approach using Craig-Bampton reduction provides better time performance than the LFB approach based on modal truncation. Both methods provide similar reductions for element processing. However, SE provides much better performance with regards to contact algorithm. In addition, rigid body handling increases drastically using the LFB.

With regards to accuracy, it was noticed that the accuracy of the model depends on the interactive nature of the reduced parts of the model. When the reduced parts were not in contact with each other, the error was more than 30% and the plots overestimated or underestimated behaviour despite having similar shapes to those of the FOM. On the other hand, when the reduced substructures presented some interactive behaviour between each other through contact, the accuracy was much better. In fact, in the studied example, the SE matched the FOM completely with only 15 EM and the LFB presented a small error. The reason behind that is linked to the extracted eigenmodes. When the substructures are not in contact, the extracted eigenmodes don't excite them simultaneously. Also, the extracted modes introduce rigid body motion of all substructures (6 per substructure). This leaves us with less useful modes, out of the total extracted ones, that can achieve accuracy. On the other hand, when the substructures are interconnected, the eigenmodes excite all of them simultaneously and less rigid body modes are present, leaving us with more useful modes. This allows us to achieve better accuracy with a smaller number of eigenmodes which eventually leads to shorter rigid body handling time and ultimately better overall time performance.

The application of the LFB linear MOR approach and the D2R approach in crash analysis led to several important observations. First, it was noticed that the computing environment influences the run time

significantly, be it the FOM or the ROM. Running a model in a practical environment doesn't guarantee that the reduction approach (LFB) and the rigid approach (D2R) would yield faster calculations.

It was also noticed that, depending on the number of CPUs used to perform a simulation, a different MPP decomposition logic may be required to achieve shorter computational times. The same decomposition logic performed differently on 4, 8, and 12 CPUs. Also, the default RCB decomposition performed well using 4 CPUs but didn't perform well using 8, 12, and 16 CPUs. The reason behind that is the load balance and communication, consequently scalability of the model, changes as the number of processors increases. The change is of course problem dependent. So, using a non-default decomposition was essential to achieving consistent times when more than 4 CPUs were used. Accordingly, it was deduced that the performance of the linear MOR method and that of the rigid-body approach highly depends on the decomposition logic and number of processors. It is believed that there is a close relation between decomposing the reduced rigid body and the overall performance. Therefore, the engineer shall invest time into finding the best decomposition for the problem in hand.

There exists a variety of things that shall be investigated in order to optimise the usage of linear MOR methods in crash analysis, in particular using LS-DYNA. A good decomposition logic shall be investigated; different special decompositions shall be tested on different numbers of processors. This would also help detect the scalability of the model. Most importantly, the decomposition of the reduced and/or rigid part(s) shall be investigated. Is it better to distribute them over all CPUs or to isolate them?

It was noticed, that when the reduced parts are originally in contact, the performance with regards to time and accuracy is better. In this work, the five reduced substructures of the Yaris model were not all in contact. It would be worth it, to test the methods using a more compact set of substructures such as the rear part of the vehicle which is not affected by the front or side crash and thus behaves linearly.

A frequency analysis can be combined with the MOR methods in order to improve accuracy. The crash introduces time varying forces which can be transformed into the frequency domain in order to obtain a frequency spectrum. These frequencies are then used as a guide to extract the eigenmodes that are activated by the most dominant frequencies. The approach followed in this work was based on extracting the first 15, 20, ... eigenmodes. However, these modes are not necessarily the ones that will be excited in the crash, hence the displacements approximated using these extracted modes would lack accuracy. LS-DYNA offers the capability of extracting modes related to frequencies located left and right to a defined central frequency. Therefore, it can be used to perform the reduction after performing a frequency analysis. According to [3], all the modes whose frequencies are up to at least two or three times the highest exciting frequency should be retained.

Since the SE approach, which can be based on static condensation or Craig-Bampton linear MOR, failed in models exhibiting large displacements, investigating other techniques to form the SE is a possibility. The system identification matrices (mass, stiffness, and inertia) of the part to be reduced can be extracted from LS-DYNA and reduced using a certain MOR software using other MOR techniques. The reduced system shall again be stored in a DMIG format, in order to be imported back into LS-DYNA.

7 Acknowledgement

The author would like to thank Ms. Jana Büttner, M.Sc. (Dr. Ing. h.c. F. Porsche AG) for her insight, feedback, and hints. These have helped ensure that this work addresses issues that are of importance in the automotive industry and therefore, added value to this work. Many thanks to SCALE GmbH, in particular Mr. Marko Thiele, for his feedback and constructive comments that also helped shape and direct this research towards the interests of the industry. Last but not least, the author would like to express his deepest gratitude and appreciation to his supervisor and mentor, Prof. Uwe Reuter. Under his supervision, a lot of new knowledge and expertise was acquired, not only scientifically but also socially.

8 Literature

- [1] Schilders, W., Van der Vorst, H., and Rommes, J.: "Model Order Reduction: Theory, Research Aspects and Applications", volume 13. Springer, Berlin, 2008.
- [2] Antoulas, A.: "Approximation of Large-Scale Dynamical Systems". Society for Industrial and Applied Mathematics, Philadelphia, PA, 2005.
- [3] Qu., Z.: "Model Order Reduction Techniques: with Applications in Finite Element Analysis". Springer-Verlag, London, 2004.

- [4] G radin, M., and Rixen, D.: "Mechanical Vibrations: Theory and Application to Structural Dynamics". John Wiley & Sons, Chichester, United Kingdom, 3 edition, 2015.
- [5] Krattiger, D., Wu, L., Zacharczuk, M., Buck, M., Kuether, R., Allen, M., Tiso, P., and Brake., M.: "Interface reduction for hurty/craig-bampton substructured models: Review and improvements". Mechanical Systems and Signal Processing, 114, 2019, 579 – 603.
- [6] Fehr, J., Holzwarth, P., and Eberhard, P.: "Interface and model reduction for efficient explicit simulations - a case study with nonlinear vehicle crash models". Mathematical and Computer Modelling of Dynamical Systems, 22(4), 2016, 380–396.
- [7] Maker, B. and Benson, D.: "Modal methods for transient dynamics analysis in LS-DYNA." Livermore Software Technology Corporation, 2002.
- [8] Livermore Software Technology Corporation. "LS-DYNA Keyword User's Manual". LSTC, Livermore, California, R11 edition, 2018.
- [9] Bitzenbauer, J., Franz, U., and Schweizerhof, K.: "Deformable rigid bodies in LS-DYNA with applications–merits and limits". In Proceedings 5th European LS-DYNA User Conference, Birmingham, UK, 2005.
- [10] Bitzenbauer, J., Franz, U., Schulz, A., and Mlekusch, B.: "Coupling of deformable rigid bodies with finite elements to simulate FMVSS head impact". In Proceedings 4th LSDYNA User Conference, Bamberg, Germany, 2005.
- [11] Center for Collision Safety and Analysis (CCSA). "2010 Toyota Yaris detailed finite element model". <https://www.ccsa.gmu.edu/models/2010-toyota-yaris/>, 2020. [Online; accessed 20-May-2020].